

Studies of light mesons at COMPASS

Sebastian Uhl^{1,a,b}, on behalf of the COMPASS Collaboration

¹ *Technische Universität München, James-Frank-Straße, 85748 Garching, Germany*

Abstract. To investigate the spectrum of light mesons, the COMPASS experiment has recorded data with a 190 GeV/c negative pion beam impinging on a liquid hydrogen target. Diffractive dissociation reactions at squared four-momentum transfers to the target between 0.1 and 1.0 (GeV/c)² are studied. The flagship channel is the $\pi^- \pi^+ \pi^-$ final state, for which COMPASS has recorded the at present world's largest data sample. A new axial-vector signal, the $a_1(1420)$, has been found with unusual properties, pointing to an exotic nature. The findings are confirmed by the analysis of the $\pi^- \pi^0 \pi^0$ final state.

1 Introduction

The **Common Muon and Proton Apparatus for Structure and Spectroscopy** (COMPASS) experiment is a fixed-target experiment located at CERN's Super Proton Synchrotron (SPS). One of its goals is to study the spectrum of light mesons. A 190 GeV/c negative hadron beam, consisting mostly of pions with a small admixture of kaons and anti-protons, impinges on a liquid hydrogen target, and diffractively produces the mesons under study. The decay products of these mesons are detected in a two-stage magnetic spectrometer (see figure 1). Each of the two spectrometer stages is equipped with an electromagnetic calorimeter. This setup provides nearly full phase-space coverage for charged and neutral particles, resulting in a homogenous acceptance over a wide kinematic range [1].

The reaction under study here is the diffractive production of mesons decaying either into the $\pi^- \pi^- \pi^+$ or the $\pi^- \pi^0 \pi^0$ final state. To this end, exclusive events with a squared four-momentum transfer to the target t' between 0.1 (GeV/c)² and 1.0 (GeV/c)² have been selected in a three-pion mass range between 0.5 GeV/c² and 2.5 GeV/c². The selected dataset consists of 50 million $\pi^- \pi^- \pi^+$ and 3.5 million $\pi^- \pi^0 \pi^0$ events. The invariant mass distributions of the two final states indicate a rich spectrum of contributing states (see figure 2).

2 Partial-wave analysis

To decompose the three-pion mass spectra into individual spin-parity components, a partial-wave analysis employing the isobar model is used. Figure 3 sketches the process under study. The beam

^ae-mail: sebastian.uhl@mytum.de

^bThe author acknowledges support by the German Bundesministerium für Bildung und Forschung (BMBF), by the Maier-Leibnitz-Laboratorium der Universität und der Technischen Universität München, by the DFG Cluster of Excellence "Origin and Structure of the Universe" (Exc153), and by the computing facilities of the Computational Center for Particle and Astrophysics (C2PAP).

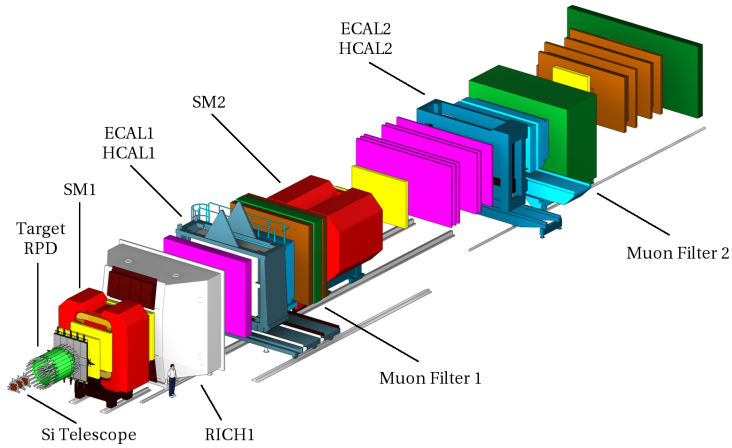


Figure 1. Sketch of the experimental setup. The beam enters the experiment from the lower left corner of the figure. (Figure from [1].)

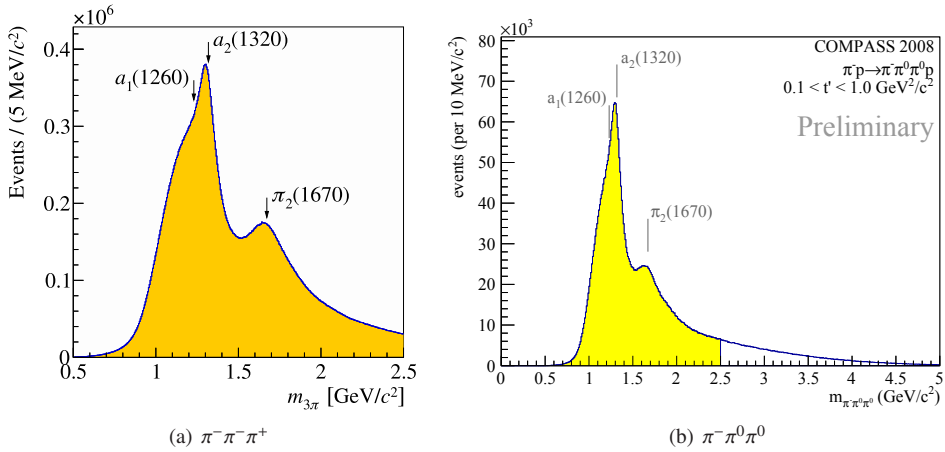


Figure 2. Invariant mass spectra of the two studied final states. (Figure (a) from [2].)

π^- diffractively scatters off the target proton producing an intermediate state X^- , which subsequently decays into a two-pion isobar $R_{\pi\pi}$ and a bachelor pion with a relative orbital angular momentum L . The isobar then decays into two pions. By exploiting the distribution in the five phase-space variables that define the kinematics of the decay products at a given invariant mass of the three-pion state, information on the spin J , the parity P , and the spin-projection M of X^- , and on the naturality ε of the exchange particle can be extracted [2].

The mass spectra of the two-pion subsystems of the $\pi^- \pi^0 \pi^0$ final state are shown in figure 4. The isobars decaying to $\pi^- \pi^0$ have isospin $I = 1$. The $\rho(770)$ is clearly visible in figure 4(a). A smaller

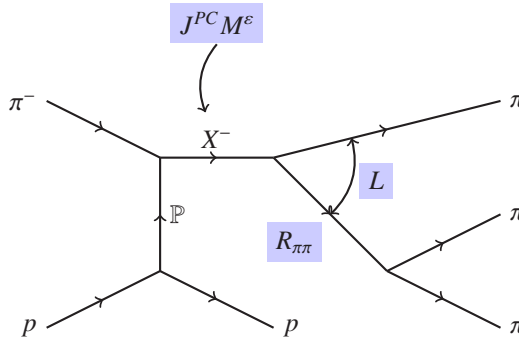


Figure 3. Sketch of the process under study.

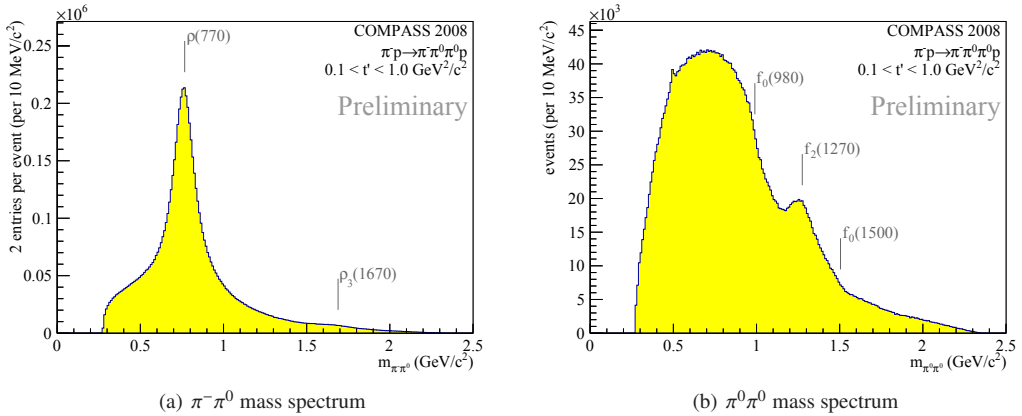


Figure 4. Invariant mass spectra of the two possible two-pion subsystems of the $\pi^- \pi^0 \pi^0$ final state.

shoulder at higher masses suggests to also use the ρ_3 (1690) as an isobar in the partial-wave analysis model. The $\pi^0 \pi^0$ isobars have isospin $I = 0$. Here, the f_0 (980), the f_2 (1270), and the f_0 (1500) are identified by bumps and kinks on top of a broad $\pi\pi$ S -wave component $(\pi\pi)_S$ in figure 4(b). For the $\pi^- \pi^- \pi^+$ final state, the two different isospin contributions cannot be separated and appear both in the $\pi^- \pi^+$ subsystem. The same isobars as for the $\pi^- \pi^0 \pi^0$ final state are used in the partial-wave analysis.

Each partial wave in the partial-wave model corresponds to a state X^- with quantum numbers $J^{PC} M^\epsilon$ decaying via a particular decay chain $R_{\pi\pi} \pi L$. For the analyses presented in the following, waves with spin J up to 6 are included. Also the orbital angular momentum L between the isobar $R_{\pi\pi}$ and the bachelor pion can go up to 6. Out of the possible combinations, 87 waves with non-negligible intensity are kept for the final model: 80 waves with a positive naturality $\epsilon = +1$ of the exchange particle and 7 with $\epsilon = -1$. In addition, one incoherent wave with an isotropic angular distribution is included [2]. The same set of 88 partial waves is used in the two analyses of the different three-pion final states.

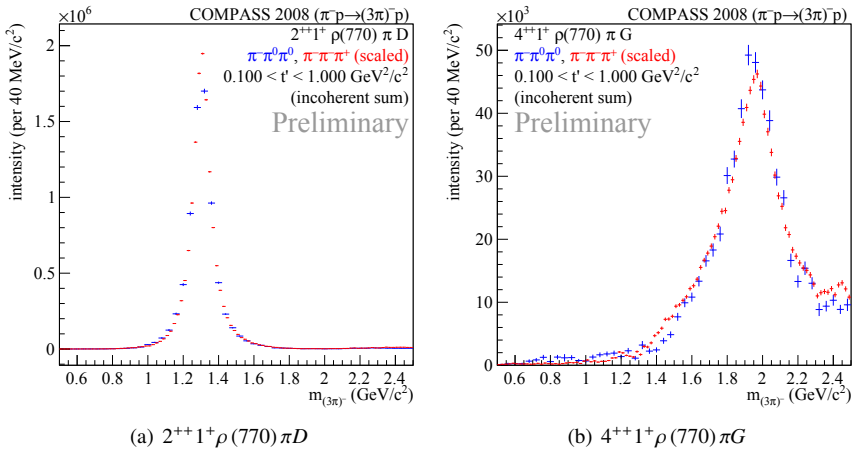


Figure 5. Sum of partial-wave intensities over all t' bins.

3 Spin-parity Decomposition

As a first analysis step, the partial-wave amplitudes are extracted in bins of the three-pion mass and the squared four-momentum transfer t' to the target assuming that all waves are fully coherent (rank-1 fit). Figure 5 shows the sum of the intensities over the individual t' bins for the $2^{++}1^+ \rho(770) \pi D$ wave, clearly showing the $a_2(1320)$, and for the $4^{++}1^+ \rho(770) \pi G$ wave, clearly showing the $a_4(2040)$. The results from the $\pi^- \pi^+ \pi^0$ channel (red markers) and the $\pi^- \pi^0 \pi^+$ channel (blue markers) are in agreement. The two data sets are normalized using the intensity integrals in each individual plot so that the peak shapes can directly be compared. As expected, no dependence of the peak shapes on t' is observed for these two partial waves. Good agreement of the partial-wave intensities between the two final states is also found for other waves with large intensities, like e.g. the $1^{++}0^+ \rho(770) \pi S$ and $2^- 0^+ f_2(1270) \pi S$ waves [3].

Also for waves with small intensities good agreement between the two final states is observed. One particularly interesting signal is observed in the $1^{++}0^+ f_0(980) \pi P$ wave around 1.4 GeV/c² (see figure 6). This narrow structure, never observed before, could correspond to a possible new a_1 state. It is seen in the decay via the $f_0(980)$ isobar for both channels and for all t' bins. Different parameterizations for the isobars have been tested to exclude possible artifacts from the employed model.

For a resonant interpretation of this signal, in addition to the intensities, also the phase difference between partial waves needs to be considered. Figure 7 shows the phase difference between the $1^{++}0^+ f_0(980) \pi P$ and the $4^{++}1^+ \rho(770) \pi G$ wave. A clear rapidly rising phase motion is visible around 1.4 GeV/c² at the position of the peak in the intensity spectrum.

In order to exclude possible artifacts caused by the particular choice for the parametrization of the isoscalar $J^{PC} = 0^{++}$ isobars, a partial-wave analysis was performed, in which the waves with broad $(\pi\pi)_S$, $f_0(980)$, and $f_0(1500)$ isobars are replaced by a set of amplitudes that are piecewise constant in the two-pion mass [2]. This novel approach allows for a rather model-independent extraction of the 0^{++} isobar amplitudes as function of the invariant mass of the three-pion system and its quantum numbers. The analysis shows a clear correlation between the new $a_1(1420)$ signal and the $f_0(980)$ as a decay product.

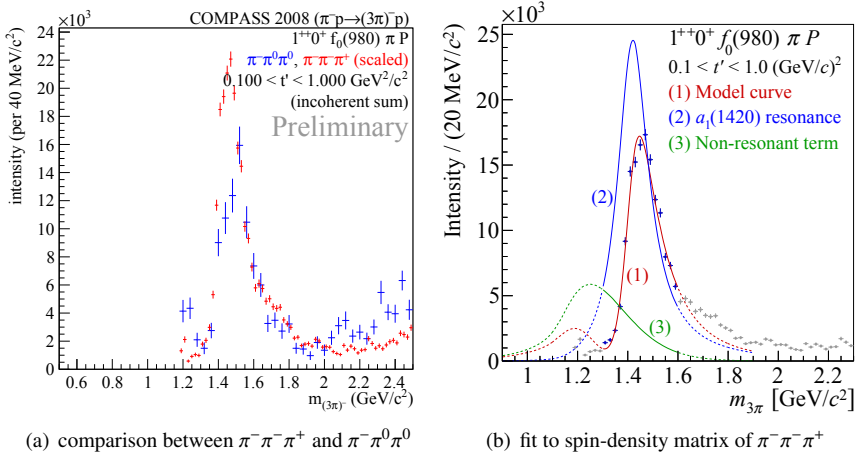


Figure 6. Sum of partial-wave intensities over all t' bins of the $1^{++}0^+ f_0(980) \pi P$ wave. (Figure (b) from [4].)

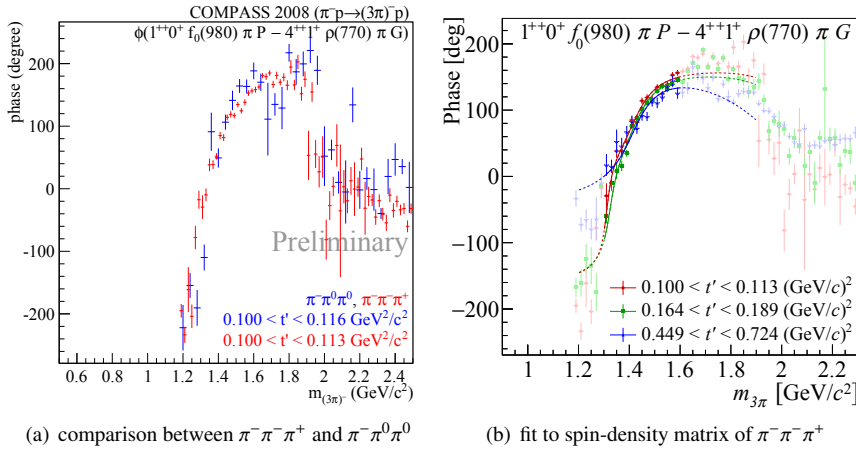


Figure 7. Phase difference between the $1^{++}0^+ f_0(980) \pi P$ and the $4^{++}1^+ \rho(770) \pi G$ wave (a) for the lowest t' bins of the $\pi^- \pi^- \pi^+$ and $\pi^- \pi^0 \pi^0$ final states, and (b) for different t' bins of the $\pi^- \pi^- \pi^+$ final state overlaid with the result of a fit to the spin-density matrix. (Figure (b) from [4].)

4 Resonance-model fit to spin-density matrix

To further study this new signal, and to extract Breit-Wigner parameters, the mass dependence of a sub-set of the spin-density matrix was extracted for the $\pi^- \pi^- \pi^+$ channel [4]. In addition to the intensities, also the interferences between the waves were taken into account. The three waves shown in figures 5 and 6 were used. The resonance model includes one Breit-Wigner resonance in each wave: the $a_2(1320)$ in the $2^{++}1^+ \rho(770) \pi D$ wave, the $a_4(2040)$ in the $4^{++}1^+ \rho(770) \pi G$ wave, and a new $a_1(1420)$ in the $1^{++}0^+ f_0(980) \pi P$ wave. The Breit-Wigner parameters were extracted by simultaneously fitting the spin-density submatrices of the three partial waves in all eleven t' bins. In addition

to the Breit-Wigner components used to describe the resonances, also a coherent t' -dependent non-resonant contribution was allowed in each wave. The parameters of the Breit-Wigner functions and of the coherent backgrounds were the same in all t' bins, only the complex-valued couplings were allowed to change with t' .

The partial-wave intensity of the $1^{++}0^+ f_0(980) \pi P$ wave (blue markers in figure 6(b)) is described by a resonant contribution for the new $a_1(1420)$ (blue curve) interfering with a non-resonant contribution (green curve). The total intensity of the model is represented by the red curve. The fit range is indicated by the continuous curve, the dashed curve shows the extrapolation of the model. Figure 7(b) shows the interference between the $1^{++}0^+ f_0(980) \pi P$ and the $4^{++}1^+ \rho(770) \pi G$ wave. The three different colors represent three of the in total eleven t' bins. Again, the markers show the result from the partial-wave decomposition, while the curves show the behaviour of the resonance model. The parameters of the Breit-Wigner amplitude describing the new $a_1(1420)$ are $M = 1414 \text{ MeV}/c^2$ with a systematic uncertainty of $^{+15}_{-13} \text{ MeV}/c^2$ for the mass, and $\Gamma = 153 \text{ MeV}/c^2$ with a systematic uncertainty of $^{+8}_{-23} \text{ MeV}/c^2$ for the width. The statistical uncertainties are negligible.

5 Conclusions

The COMPASS experiment has recorded a large dataset to study excited light-quark resonances produced in diffractive dissociation into three pions. The large number of events allowed us to increase the number of waves used in the partial-wave analysis. In addition, the analysis is performed in narrow bins of t' . Breit-Wigner parameters have been extracted by performing a resonance-model fit to the result of the spin-parity decomposition in mass bins. Apart from the well-known resonances, COMPASS found a new signal in the $1^{++}0^+ f_0(980) \pi P$ wave around $1.4 \text{ GeV}/c^2$. It is a rather narrow object with a well-defined mass and width, and appears only in the $f_0(980)$ decay mode. The nature of this signal is still unclear, it could be the isospin partner of the $f_1(1420)$, but also other explanations have been put forward. The $a_1(1420)$ could be a genuine resonance in the form of a two-quark-tetraquark mixed state [5] or a tetraquark with mixed flavor symmetry [6]. Also two explanations connecting the new $a_1(1420)$ to the known $a_1(1260)$ have been proposed. The first explains the observed intensity spectra and phases in the $1^{++}0^+ f_0(980) \pi P$ wave by a two-channel unitarized Deck amplitude interfering with the direct production of the $a_1(1260)$ [7]. The second explains the signal by a singularity in a triangle diagram describing rescattering in the $K^- \bar{K}^*$ decay of the $a_1(1260)$ [8, 9].

References

- [1] COMPASS collaboration, P. Abbon *et al.*, NIM **A779**, 69 (2015), arXiv:1410.1797.
- [2] COMPASS collaboration, C. Adolph *et al.*, submitted to Phys. Rev. D, arXiv:1509.00992.
- [3] S. Uhl on behalf of the COMPASS Collaboration, PoS(Hadron 2013)087, arXiv:1401.4943.
- [4] COMPASS collaboration, C. Adolph *et al.*, Phys. Rev. Lett. **115**, 082001 (2015), arXiv:1501.05732.
- [5] Z.G. Wang, arXiv:1401.1134.
- [6] H.X. Chen *et al.*, Phys. Rev. **D91**, 094022 (2015).
- [7] J.L. Basdevant, E. Berger, Phys. Rev. Lett. **19**, 192001 (2015).
- [8] M. Mikhasenko, B. Ketzer, A. Sarantsev, Phys. Rev. **D91**, 094015 (2015).
- [9] F. Aceti, L.R. Dai, E. Oset, arXiv:1606.06893.